AGU PUBLICATIONS

JGR

Journal of Geophysical Research: Space Physics

RESEARCH ARTICLE
10.1002/2015JA021968

EMIC waves observed at geosynchronous orbit under quiet geomagnetic conditions ($Kp \leq 1$)

J.-S. Park[1], K.-H. Kim[2,3], K. Shiokawa[3], D.-H. Lee[2], E. Lee[2], H.-J. Kwon[4], H. Jin[2], and G. Jee[4]

[1]Institute of Space Science, National Central University, Jhongli, Taiwan, [2]School of Space Research, Kyung Hee University, Yongin, South Korea, [3]Institute for Space-Earth Environmental Research, Nagoya University, Nagoya, Japan, [4]Korea Polar Research Institute, Incheon, South Korea

Key Points:
- EMIC waves under quiet geomagnetic conditions
- EMIC occurrence peak near noon
- Solar wind dynamic pressure variation is a major factor for quiet time EMIC wave generation

Correspondence to:
K.-H. Kim,
khan@khu.ac.kr

Citation:
Park, J.-S., K.-H. Kim, K. Shiokawa, D.-H. Lee, E. Lee, H.-J. Kwon, H. Jin, and G. Jee (2016), EMIC waves observed at geosynchronous orbit under quiet geomagnetic conditions ($Kp \leq 1$), *J. Geophys. Res. Space Physics*, *121*, 1377–1390, doi:10.1002/2015JA021968.

Received 30 SEP 2015
Accepted 28 JAN 2016
Accepted article online 1 FEB 2016
Published online 27 FEB 2016

Abstract We statistically study the local time distribution of the helium band electromagnetic ion cyclotron (EMIC) waves observed at geosynchronous orbit when geomagnetic activity was low ($Kp \leq 1$). In order to identify the geosynchronous EMIC waves, we use high time resolution magnetic field data acquired from GOES 10, 11, and 12 over a 2 year period from 2007 and 2008 and examine the local time distribution of EMIC wave events. Unlike previous studies, which reported high EMIC wave occurrence in the postnoon sector with a peak around 1500–1600 magnetic local time (MLT) during magnetically disturbed times (i.e., storm and/or substorm), we observed that quiet time EMIC waves mostly occur in a region from morning (~0600 MLT) to afternoon (~1600 MLT) with a peak around 1100–1200 MLT. To investigate whether the quiet time EMIC wave occurrence has a causal relationship with magnetospheric convection enhancement or solar wind dynamic pressure variations, we performed a superposed epoch analysis of solar wind parameters (solar wind speed, density, dynamic pressure, and interplanetary magnetic field B_z) and geomagnetic indices (*AE* and *SYM-H*). From the superposed epoch analysis we found that solar wind dynamic pressure variation is a more important parameter than *AE* and *SYM-H* for quiet time EMIC wave occurrence.

1. Introduction

Electromagnetic ion cyclotron (EMIC) waves have been detected over a wide *L* range and at most local times in the Earth's magnetosphere in the Pc1–Pc2 (0.1–5 Hz) frequency range [e.g., *Anderson et al.*, 1992; *Fraser and Nguyen*, 2001; *Min et al.*, 2012; *Usanova et al.*, 2012; *Keika et al.*, 2013]. Since EMIC waves strongly affect the dynamics of ring current and radiation belt particles, leading to plasma heating and/or precipitation loss through resonant wave-particle interactions [e.g., *Thorne and Kennel*, 1971; *Erlandson and Ukhorskiy*, 2001; *Summers and Thorne*, 2003; *Miyoshi et al.*, 2008; *Yuan et al.*, 2012; *Hyun et al.*, 2014], it is important to understand the properties of EMIC waves, i.e., how and where they are generated and enhanced.

EMIC waves are typically excited as left-hand polarized waves through a cyclotron resonant interaction with ~10–100 keV anisotropic ($T_\perp > T_\parallel$) ions to provide free energy for instability, where $T_\perp$ and $T_\parallel$ are temperatures, respectively, perpendicular and parallel to the background magnetic field [e.g., *Cornwall*, 1965; *Kennel and Petschek*, 1966; *Young et al.*, 1981; *Roux et al.*, 1982]. Such anisotropic conditions may be expected when magnetospheric convection is enhanced or when the magnetosphere is compressed by strong solar wind dynamic pressure enhancement [e.g., *McCollough et al.*, 2010]. Thus, many publications have focused on the EMIC wave events occurring during geomagnetically disturbed intervals associated with geomagnetic storms and substorms [e.g., *Fraser and McPherron*, 1982; *Ishida et al.*, 1987; *Erlandson and Ukhorskiy*, 2001; *Meredith et al.*, 2003; *Fraser et al.*, 2010; *Halford et al.*, 2010] and interplanetary shocks [e.g., *Olson and Lee*, 1983; *Anderson and Hamilton*, 1993; *Arnoldy et al.*, 2005; *Usanova et al.*, 2008].

Theoretical studies have shown that the equatorial region of the magnetosphere is favored for EMIC wave generation because of low group velocity of the wave in that region, leading to enhancement of convective growth rate [e.g., *Cornwall*, 1965; *Kennel and Petschek*, 1966]. Since the growth rate and amplification of EMIC waves are controlled by the parallel temperature, the temperature anisotropy of energetic ion population, the ion composition, and the cold plasma density [e.g., *Kozyra et al.*, 1984; *Horne and Thorne*, 1994; *Hu and Fraser*, 1994], it is important to understand the dynamics of both the plasmasphere and ring current ions.

Previous statistical studies reported that EMIC waves are most frequently observed in the postnoon magnetic local time (MLT) sector at a wide L range from the inner magnetosphere to the outer magnetosphere [*Anderson et al.*, 1992; *Fraser and Nguyen*, 2001; *Meredith et al.*, 2003; *Clausen et al.*, 2011; *Min et al.*, 2012; *Usanova et al.*, 2012; *Keika et al.*, 2013]. It has been suggested that the occurrence peak at postnoon is strongly associated with the region where energetic ring current ions injected from the plasma sheet overlap near the dusk sector with the cold plasma population of the plasmaspheric bulge and plumes.

Since the dynamic behavior of the plasmapause is strongly influenced by the solar-wind-driven electric field, the cold plasmaspheric plasmas in drainage plumes extending out from the plasmapause and plasmaspheric bulge are expected to be in the postnoon sector including the duskside sector during intervals of enhanced magnetospheric convection (i.e., storm times associated with strong southward interplanetary magnetic field intervals) [e.g., *Spasojević et al.*, 2003; *Goldstein et al.*, 2004; *Kim et al.*, 2007]. It has been reported that plasma plumes or bulge in the postnoon sector may contribute to enhanced EMIC wave activity just inside geosynchronous orbit [*Halford et al.*, 2010] and at geosynchronous orbit [*Fraser et al.*, 2010] during storm times.

Under quiet geomagnetic conditions, it is expected that the Earth's corotational electric field dominates convection plasma flows as magnetospheric convection becomes weak. This causes the plasmapause to expand beyond the typical location of the plasmapause at $L = 4–5$ [*O'Brien and Moldwin*, 2003]. Recently, *Kwon et al.* [2015] reported that the quiet time plasmapause is located near geosynchronous orbit nearly independent of MLT. Thus, the spatial distribution of EMIC waves occurring under quiet geomagnetic conditions may be different from that during disturbed geomagnetic intervals.

In this paper, we investigate the local time distribution of the EMIC wave occurrence rate at geosynchronous orbit under quiet geomagnetic conditions ($Kp \leq 1$). We note that the properties of quiet time EMIC waves have been previously reported by *Usanova et al.* [2012]. They statistically examined quiet time EMIC waves using Time History of Events and Macroscale Interactions during Substorms (THEMIS) data obtained over a wide range of $L = 3–10$. In their study, the MLT dependence of EMIC wave occurrence rate was examined in the 6 h local time range for dawn (0300–0900 MLT), noon (0900–1500 MLT), dusk (1500–2100 MLT), and midnight (2100–2400 MLT). In this study, on the other hand, the magnetic field data from the GOES geosynchronous satellites provide sufficient statistics, allowing the smaller MLT bins. We show that quiet time EMIC waves mostly occur on the dayside with a peak occurrence near noon. This result is similar to that reported by *Usanova et al.* [2012], but the previous study did not provide the peak occurrence location in the dayside because of large local time bin. Thus, we believe that our analyses provide more quantitative evaluation for the occurrence distribution of quiet time EMIC waves at geosynchronous orbit.

This paper is organized as follows. In section 2 we describe the data and event selection procedure with examples of quiet time EMIC waves. In section 3 we present the statistical analysis. Section 4 discusses the statistical results, and conclusions are presented in section 5.

2. Data

2.1. Data Set

We identify EMIC waves using high time resolution (~0.512 s) magnetic field data acquired by the GOES 10, GOES 11, and GOES 12 spacecraft at geosynchronous orbit [*Singer et al.*, 1996] over a 2 year period from January 2007 to December 2008. GOES 10 was located at 60°W geographic longitude and a magnetic latitude (MLAT) of ~6–13°, GOES 11 at 135°W and ~4–5° in MLAT, and GOES 12 at 75°W and ~9–11° in MLAT. The high-resolution data are resampled at 0.6 s intervals, corresponding to a Nyquist frequency of ~830 mHz. The field data have been rotated into a mean-field-aligned (MFA) coordinate system in which $\hat{\mathbf{e}}_z$ is along $\hat{\mathbf{B}}_0$, $\hat{\mathbf{e}}_y$ (eastward) is parallel to $\hat{\mathbf{e}}_z \times \mathbf{r}$, where $\mathbf{r}$ is the spacecraft position vector relative to the center of the Earth, and $\hat{\mathbf{e}}_x$ (radial) is given by $\hat{\mathbf{e}}_x = \hat{\mathbf{e}}_y \times \hat{\mathbf{e}}_z$. Here $\hat{\mathbf{B}}_0$ is defined to be the low-pass-filtered magnetic field measured using 300 s moving average. Since the polarization of EMIC waves is expected to be mainly transverse, the transverse ($\hat{\mathbf{e}}_x$ and $\hat{\mathbf{e}}_y$) components of the rotated magnetic field will be used for the wave identification.

EMIC waves can be generated in three distinct bands [e.g., *Young et al.*, 1981]; H band between the local proton gyrofrequency (Ω_{H^+}) and local helium ion gyrofrequency (Ω_{He^+}), He band between the local Ω_{He^+} and local oxygen ion gyrofrequency (Ω_{O^+}), and O band below the local Ω_{O^+}. The typical quiet time magnetic field strength of ~110 nT at geosynchronous orbit provides local gyrofrequencies of Ω_{H^+} = ~1680 mHz, Ω_{He^+} = ~420 mHz, and Ω_{O^+} = ~105 mHz, respectively. The Nyquist frequency of ~830 mHz is high enough for capturing the EMIC waves in He band (~105 mHz $\leq f <$ ~420 mHz) and O band ($f <$ ~105 mHz) at geosynchronous

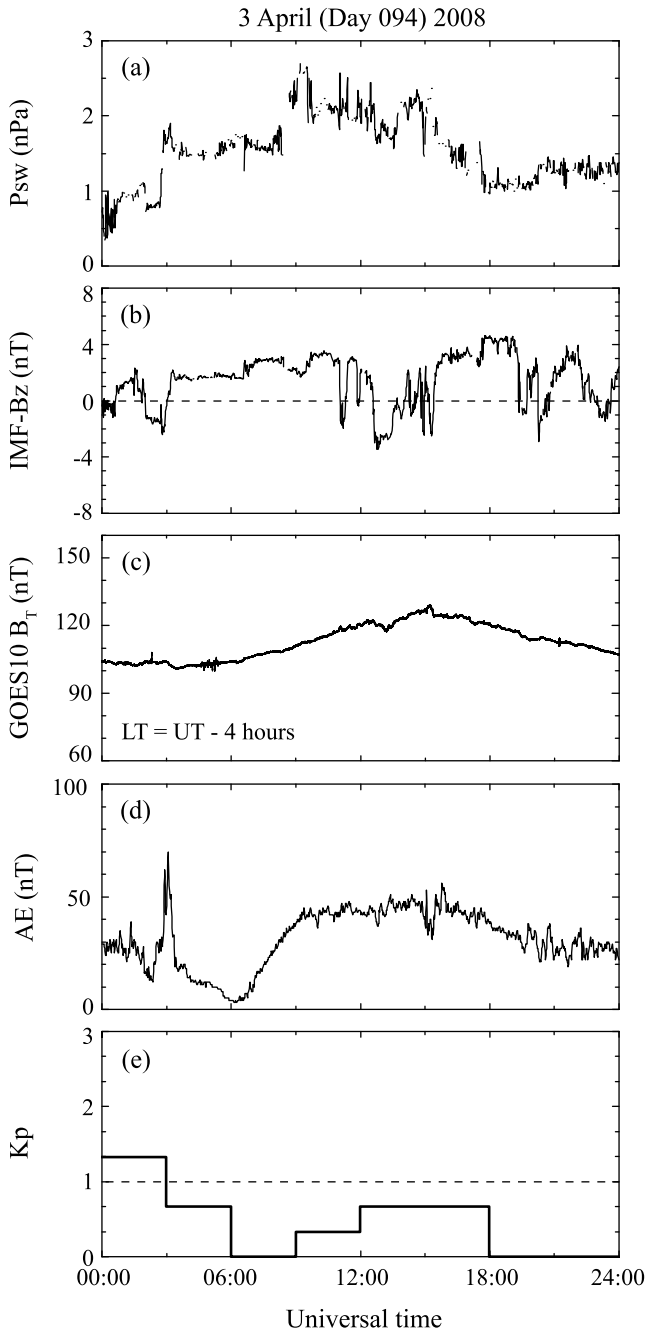

Figure 1. (a) Solar wind dynamic pressure. (b) Interplanetary magnetic field (IMF) B_z in GSM coordinates. (c) Magnetic field strength measured by GOES 10. (d) *AE* index. (e) *Kp* index.

orbit, but not for the waves in the H band. The O band of geosynchronous EMIC waves overlaps with the broad band noise in the Pc3 frequency band (~20–100 mHz). Thus, we limit our analysis to the He band EMIC waves at geosynchronous orbit in this study.

To monitor geomagnetic conditions, we use the 3 h *Kp*, 1 min *AE*, and 1 min *SYM-H* indices provided by World Data Center C2 for Geomagnetism, Kyoto University (http://wdc.kugi.kyoto-u.ac.jp/index.html). The solar wind and interplanetary magnetic field (IMF) data from OMNI Web (http://omniweb.gsfc.nasa.gov/) are used to examine external solar wind and IMF conditions for EMIC wave intervals. The OMNI data have been time shifted to the bow shock nose [*King and Papitashvili*, 2006] and provided in 1 min time resolution.

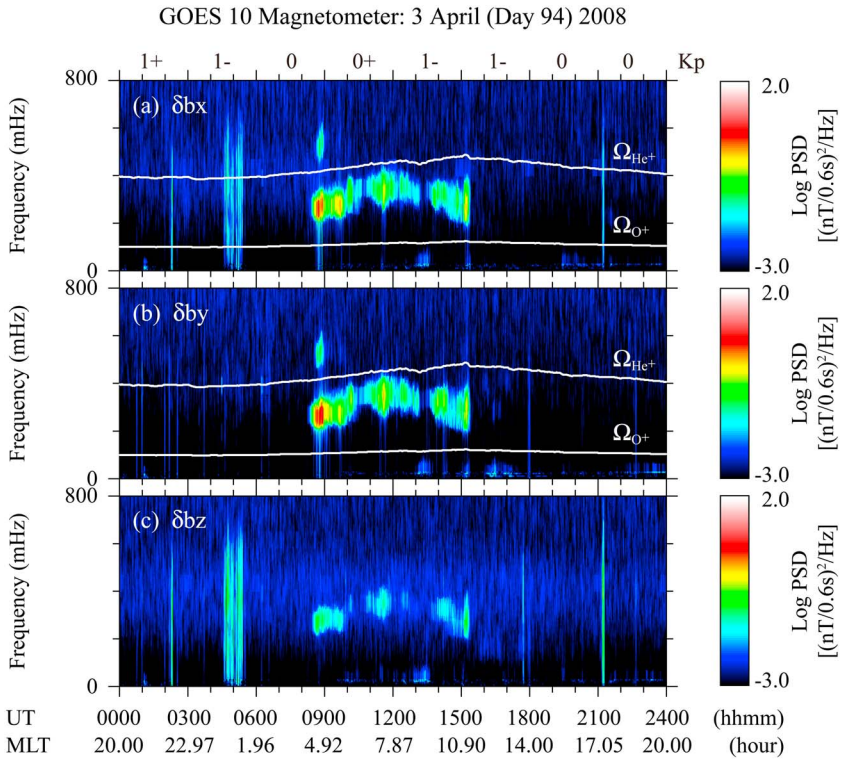

Figure 2. Dynamic power spectra for the GOES 10 magnetic field data on 3 April 2008. The 3 h *Kp* values are displayed on the top of Figure 2a. (a) δb_x, (b) δb_y, and (c) δb_z indicate perturbations in the radial, eastward, and field-aligned directions in MFA coordinate system, respectively. The data were time differenced prior to spectral estimate in order to remove a slowly varying background. Two white lines in Figures 2a and 2b indicate the local helium (Ω_{He^+}) and oxygen (Ω_{O^+}) gyrofrequencies, respectively. The magnetic local times of GOES 10 are shown at the bottom.

2.2. Examples of Quiet Time EMIC Waves and He Band EMIC Wave Selection

Figures 1a–1e show the solar wind dynamic pressure (P_{sw}), the interplanetary magnetic field (IMF) B_z, the total magnetic field strength at GOES 10, the *AE* index, and *Kp* index on 3 April 2008. P_{sw} exhibits a sudden change from ~0.8 nPa to ~1.8 nPa at around 03:00 UT and from ~1.5 nPa to ~2.5 nPa at around 08:30 UT. We do not see geosynchronous magnetic field responses to P_{sw} changes with the amplitude scale of the figure because of small enhancements in P_{sw}. The IMF was mainly northward ($B_z > 0$) on this day. The *AE* index was less than 50 nT for 24 h except for around 03:00 UT, and the *Kp* index stayed at low levels less than 1 for 21 h from 03:00 UT to 24:00 UT.

Figure 2 shows dynamic Fourier spectrograms generated for the 24 h interval of GOES 10 magnetometer data on 3 April 2008 in the MFA coordinate system. The 3 h *Kp* values are displayed on the top of Figure 2a. The power spectral density (PSD) of each component was computed by Fourier transforming the corresponding magnetic component with 3.0 min window (300 data points) moving in steps of 1.5 min. Prior to the Fourier transformation, the 0.6 s input time series was time differenced to "whiten" the spectra. Twelve-point moving averages are taken over frequency to smooth the spectral intensity. Strong spectral intensity in the transverse components (δb_x and δb_y) appears in the frequency band between the local Ω_{He^+} and Ω_{O^+} for the interval from ~08:00 UT to ~15:30 UT. Since the *Kp* index was 0 for 0600–0900 UT, 0+ for 0900–1200 UT, and 1– for 1200–1500 UT, these transverse waves are identified as quiet time EMIC waves excited in the He band. The compressional component (δb_z) also exhibits similar enhancements for the interval but with much lower spectral intensity.

To examine whether these EMIC waves are associated with magnetospheric convection enhancement (i.e., internal source) or P_{sw} enhancement (i.e., external source), we plot P_{sw} and *AE* index with the EMIC wave power (P_{tr}) in the He band in Figure 3. To systematically identify the He band EMIC waves, we use the following procedure. First, we computed the power spectral density, $\_PSD\delta bx(f)$ and $\_PSD\delta by(f)$, of the transverse components, and then the total transverse power ($PSD_{tr}(f)$) was calculated by adding two transverse components

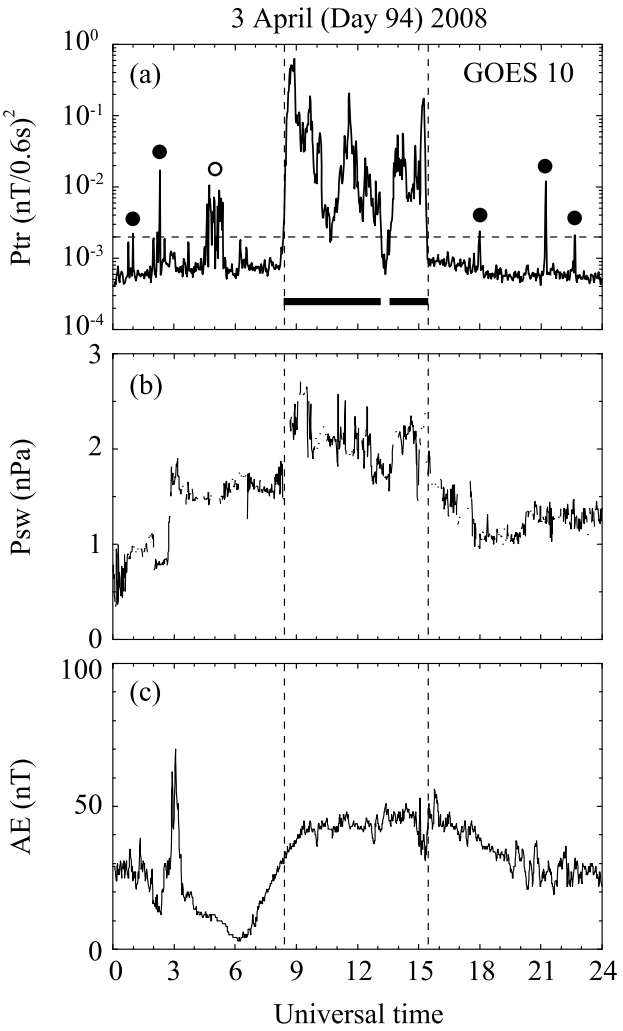

Figure 3. (a) The band-integrated EMIC wave power of the transverse components between Ω_{He^+} and Ω_{O^+} measured by GOES 10 on 3 April 2008. (b) Solar wind dynamic pressure. (c) *AE* index. The horizontal bars in Figure 3a indicate the intervals of selected quiet time EMIC wave events. Open and solid circles indicate instrumental artifacts.

of the *PSD*. The calculation was done continuously by moving a 180 s time-differenced data window (300 data points at 0.6 s time resolution) in 90 s steps for the 24 h interval regardless of the presence of EMIC wave activity. Finally, P_{tr} was obtained by integrating the power spectral density, $PSD_{tr}(f)$, over the local He band frequency range from Ω_{O^+} to Ω_{He^+}. Consequently, the samples of P_{tr} plotted in Figure 3a are at 90 s intervals.

We impose an additional condition to ensure sufficient wave power with a threshold value of 0.002 in the unit of (nT/0.6 s)^2 for P_{tr}, indicated by the horizontal dashed line in Figure 3a. After examining dynamic spectra and P_{tr} samples for all orbits, we found that the threshold value of 0.002 (nT/0.6 s)^2 is reasonable to distinguish between EMIC wave activity and background level. Although a sample of P_{tr} passes our threshold, in some cases it has a broadband spectral shape with a nearly constant spectral intensity, for example, in the frequency band from ~0 to ~600 mHz between ~04:35 and ~05:24 UT, as shown in Figure 2. Such a broadband spectrum may occur as a result of an instrumental artifact. In Figure 3a, such a signature is shown as an isolated spike (marked by solid circles) or detected continuously (marked by open circle). These non-EMIC wave activities can be easily distinguished by comparing the magnetic field dynamic spectra and a trace of P_{tr} samples. In our study one event is defined when EMIC wave activity lasts more than 10 min (i.e., more than seven samples of P_{tr}), and each event should be separated by more than 10 min.

Using the selection procedure described above, we identified two EMIC wave events marked by horizontal bars below the P_{tr} trace in Figure 3a. Two vertical dashed lines indicate the start time of the former event and

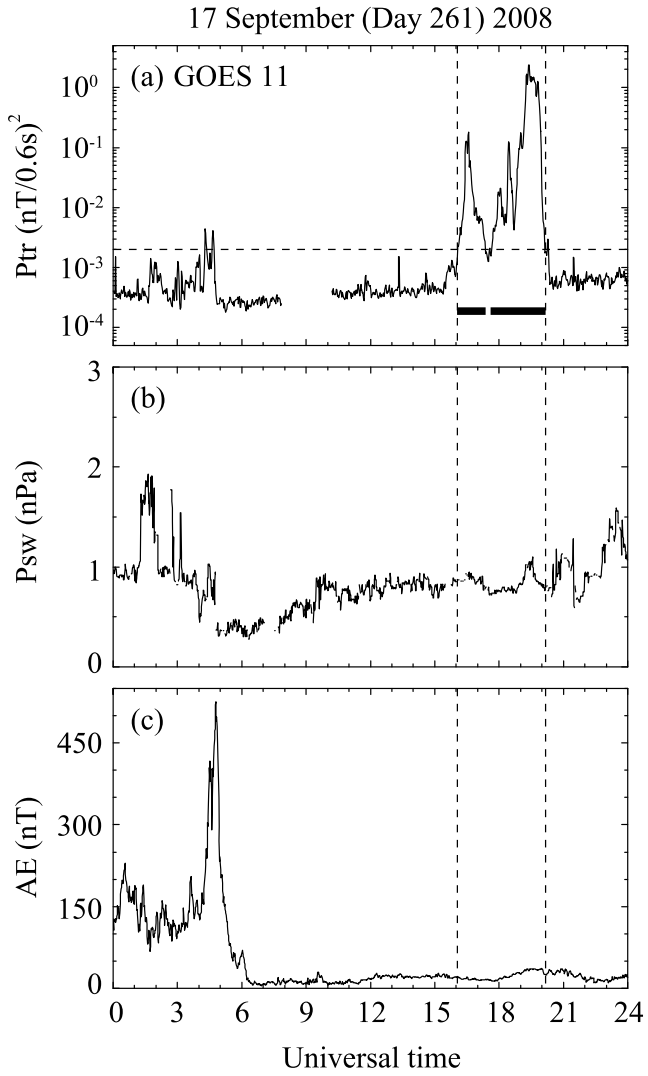

Figure 4. The format is the same as in Figure 3 except for the GOES 11 magnetic field data on 17 September 2008.

the end time of the latter event, respectively. It is clearly shown that quiet time EMIC waves are enhanced during the interval of P_{sw} enhancement exhibited in Figure 3b and that the wave onset nearly coincides with sudden increase in P_{sw} from ~1.5 to ~2.5 nPa around 08:30 UT. In contrast, the correlation between EMIC wave onset and the *AE* index variation is not so clear. That is, the EMIC waves seen at geosynchronous orbit were not associated with substorm signatures [*Ishida et al.*, 1987]. This implies that the generation of EMIC waves is the result of an external source (i.e., P_{sw} variations). Recently, similar observations at geosynchronous orbit during geomagnetically quiet times were reported by *Hyun et al.* [2014]. It has been well known that EMIC wave onset and intensification are associated with sudden impulse (SI) events [e.g., *Olson and Lee*, 1983; *Anderson and Hamilton*, 1993; *Engebretson et al.*, 2002; *Arnoldy et al.*, 2005; *Usanova et al.*, 2008]. However, we note that the P_{sw} enhancement, ΔP_{sw}, causing the onset of our quiet time EMIC waves is much smaller than that causing SI events. In addition, while there was a sudden increase in P_{sw} around 03:00 UT, no EMIC wave activity at GOES 10 was present. This may be due to the spacecraft position located near midnight. It has been reported that the dayside outer magnetosphere is a preferential location for EMIC wave activity controlled by solar wind dynamic pressure [*Usanova et al.*, 2012].

We also observed EMIC wave events that are not associated with a P_{sw} increase under quiet geomagnetic conditions. Figure 4a shows EMIC wave power enhancement detected by GOES 11 moving from 0700 to 1100 MLT for the interval of ~16:00–20:00 UT on 17 September 2008. The *Kp* index was 2+ for 00:00–06:00 UT and less than 1− for 06:00–21:00 UT. During the interval of 03:00–21:00 UT, P_{sw} showed a small variation between 0.3

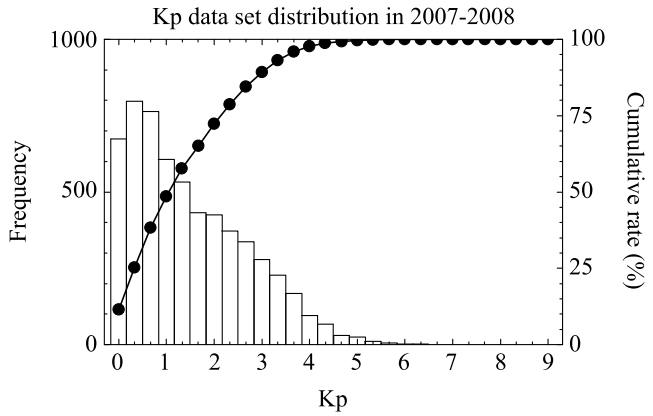

Figure 5. Occurrence frequency (histogram) distribution and cumulative rate (curve) distribution of *Kp* for 2007–2008.

and 1.0 nPa, and there was no sudden increase in P_{sw} near the onset of the EMIC wave. This indicates that the wave occurrence was not directly influenced by P_{sw} variations. The *AE* index showed a sudden increase at 04:47 UT with a peak amplitude of 526 nT, which implies substorm expansion/intensification. This sudden *AE* increase occurred 11 h prior to the EMIC wave onset. During the interval from 06:00 to 24:00 UT, *AE* was close to the base line ($AE < 50$ nT), with no indication of substorms. That is, there is no sudden enhancement in *AE* just before the wave onset, implying that the wave occurrence was not directly driven by substorm activities. However, we do not exclude that the substorm activities for the interval of 00:00–06:00 UT provided hot ion populations needed to drive the EMIC instability.

3. Statistical Analysis

In this section we statistically examine the EMIC wave events selected by the procedure described in section 2. Of 1513 EMIC wave events (493 events at GOES 10, 363 events at GOES 11, and 657 events at GOES 12) selected during the period of 2007–2008 in a solar minimum, 350 events (127 events at GOES 10, 80 events at GOES 11, and 143 events at GOES 12) occurred during quiet geomagnetic conditions with $Kp \leq 1$. Different numbers of events at GOES satellites may be due to different satellite's locations in geographic longitudes and geomagnetic latitudes. Since EMIC wave events at each GOES satellite showed a similar local time distribution, we combined three spacecraft observations for our statistical study.

Figure 5 shows the frequency distribution of the *Kp* index plotted with a histogram and its cumulative rate marked by the curve with solid circles during the period of 2007–2008 in a solar minimum. Cumulative rate provides that ~50% of this solar minimum period were under very quiet geomagnetic conditions ($Kp \leq 1$). This is due to extremely low solar activity. There was no geomagnetic activity higher than $Kp = 6+$ for the 2 year period.

Figure 6 shows the occurrence distribution of the duration times of the selected EMIC wave events for all *Kp* conditions and $Kp \leq 1$ in the 10 min bins. The absence of events in the duration time between 0 and 10 min is due to the selection criterion. That is, the event defined in our study should last more than 10 min. Note that ~1% of the events lasted more than 5 h for both *Kp* ranges (data not shown here). Two points can be found in Figure 6. One is that most EMIC waves had a duration time less than 60 min. The other is that EMIC waves tend to last slightly longer for $Kp \leq 1$ than for all *Kp* conditions at least for the duration less than 90 min.

To examine such features quantitatively, we plotted the median (solid circle) and quartile (open circle) values of the duration of EMIC wave activity as a function of *Kp* in Figure 7b with the EMIC wave occurrence in Figure 7a. The medians are distributed between 30 and 40 min with a peak of 39 min for $Kp \leq 1$. The variation of duration times, measured by the separation between the lower and upper quartiles, is greatest for $Kp \leq 1$, suggesting that EMIC waves for $Kp \leq 1$ lasted longer than those for other *Kp* values.

In order to examine how the occurrence rate of EMIC waves varies with geomagnetic disturbance level, the *Kp* distribution for the EMIC wave occurrence and the distribution of the *Kp* values are plotted in Figure 8. The occurrence distribution of *Kp* in Figure 8a shows a tendency to have higher (lower) occurrences at low (high) index levels. The number of EMIC wave events increases with increasing *Kp* by $Kp = 3$ and then decreases with

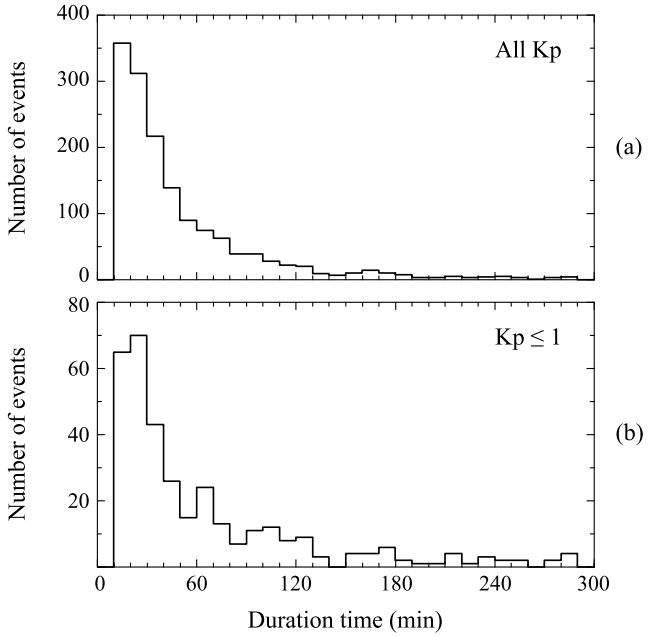

Figure 6. The number of events as a function of the duration times of the selected EMIC wave events (a) for all *Kp* conditions and (b) for $Kp \leq 1$ in the 10 min bins.

increasing *Kp*. Figure 8b shows the EMIC wave occurrence rate as a function of the *Kp* value. The occurrence rate was obtained by dividing the number of the EMIC wave events by the number of *Kp* data points for each *Kp* index level. Although the statistical significance is probably low for $Kp = 5-6$ because of the small number of samples, the overall occurrence rate of EMIC waves increases with *Kp* index. This is consistent with the result of *Usanova et al.* [2012].

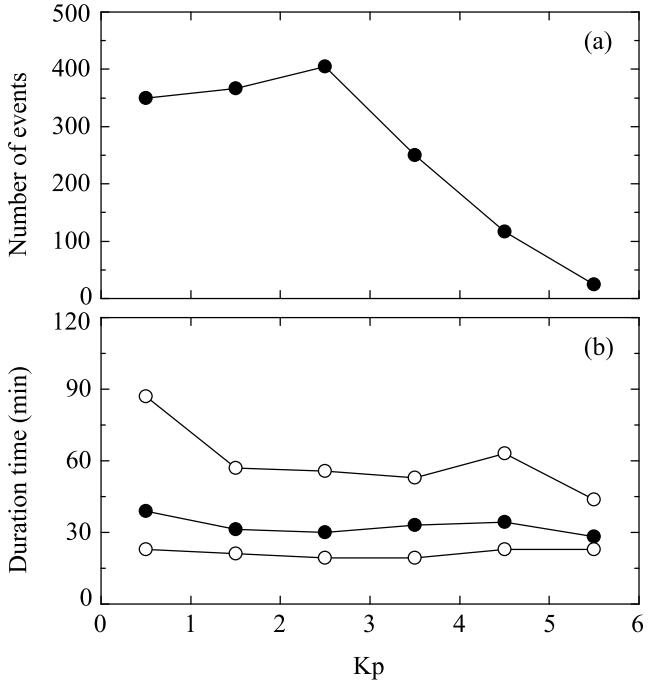

Figure 7. (a) The number of events and (b) the median (solid circle) and quartile (open circle) values of the duration of EMIC wave activity as a function of *Kp*.

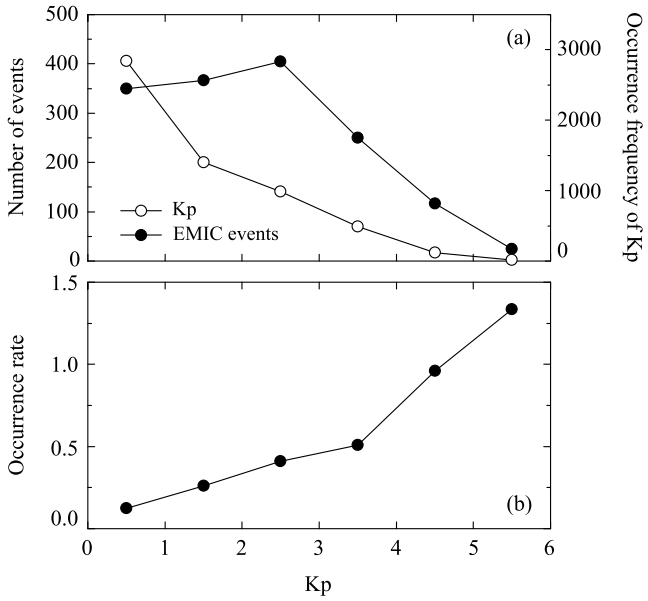

Figure 8. (a) The number of EMIC wave events (solid circles) and *Kp* occurrence frequency (open circles) as a function of *Kp* for 2007–2008. (b) The occurrence rate of wave events as a function of *Kp*. The occurrence rate was obtained by dividing the number of wave events by the number of *Kp* data points for each *Kp* index level.

Figure 9 shows the distribution of local time occurrence of the EMIC wave events for all *Kp* conditions and $Kp \leq 1$. In each panel, the red and blue traces represent the occurrence distribution for the start and end times of the events, respectively. The distribution of the event start time for all *Kp* conditions is strongly biased to the postnoon sector and has a peak around 1500–1600 MLT. The distribution of the event end time is similar to that of the start time, but it has a much broader peak around 1500–1800 MLT. Broadening may be due to the various duration times of the events. As shown in Figure 6, the majority (~73%) of the events for all *Kp*

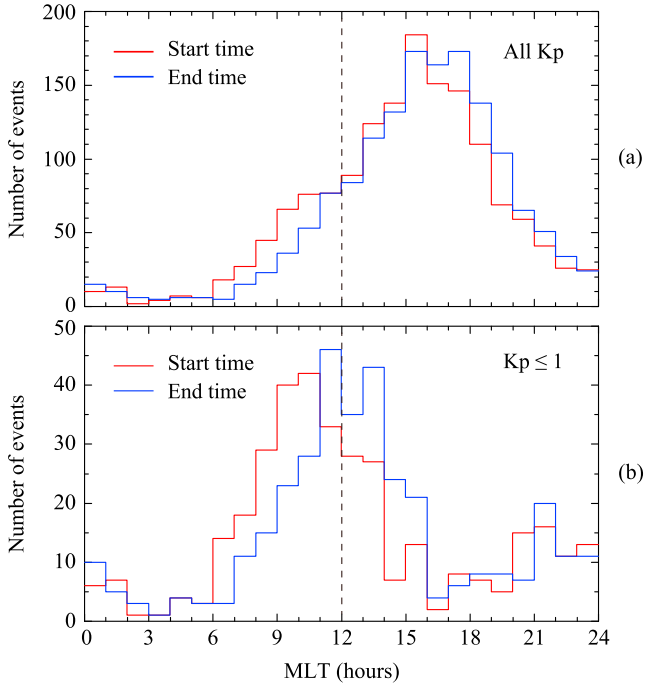

Figure 9. The local time distribution of the EMIC wave events (a) for all *Kp* conditions and (b) for $Kp \leq 1$. In each panel, the red and blue traces represent the occurrence distribution for the start and end times of the events, respectively.

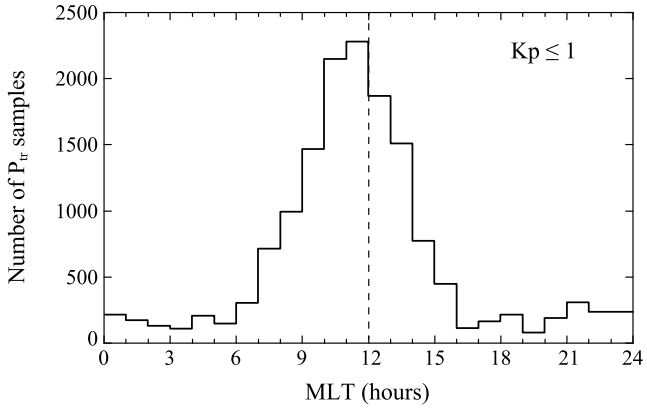

Figure 10. The local time distribution of P_{tr} samples of all events for $Kp \leq 1$.

conditions had duration times less than 1 h. This may lead to a skew of the end time distribution toward the later local times about 1 h. The local time occurrence distribution in our study is quite consistent with the results of *Clausen et al.* [2011]. Since we used the same data sets as those in *Clausen et al.* [2011], this result is not surprising. Most of the events selected in our study may be included in the statistical study by *Clausen et al.* [2011] even though the event selection procedures in both studies were different. Thus, we mainly focus on the events under quiet conditions, which were not discussed in their study.

The start time occurrence distribution for $Kp \leq 1$ shown in Figure 9b is clearly higher in the dayside, peaking in the prenoon sector (0900–1100 MLT). About 57% (199 out of 350) of the events were observed in the 0800–1400 MLT sector. In the postnoon sector (1400–1800 MLT) where high EMIC wave occurrence appears for all *Kp* conditions, the distribution of quiet time EMIC waves was very low. The distribution of the end time occurrence is skewed toward the later local times about more than 1 h with a broader peak around 1100–1400 MLT. This is due to the fact that quiet time EMIC waves lasted longer as shown in Figure 7. About 63% (220 out of 350) of the events occurred in the region of 0900–1600 MLT. This local time distribution is similar to that of periodic and narrow band Pc1–Pc2 emissions observed at geosynchronous orbit in 2007 [*Fraser et al.*, 2012].

From these observations we suggest that quiet time EMIC waves mostly occur in a region from morning to afternoon with a peak occurrence near noon. To confirm this argument, the number of P_{tr} samples of all events for $Kp \leq 1$ are plotted in Figure 10. As expected from Figure 9b, most of the P_{tr} samples occurred between ~0600 and ~1600 MLT with a peak around 1100–1200 MLT. In addition, we confirmed that the distribution of the samples bounded by 0600 and 1600 MLT is biased toward the morning side. That is, there is a morning-afternoon asymmetry in the occurrence distribution of quiet time EMIC waves at geosynchronous orbit.

4. Discussion

We observed that the EMIC wave events occur mainly in the postnoon sector with a peak around 1500–1600 MLT for all *Kp* conditions (see Figure 9a). This high occurrence rate of EMIC waves in that region has been reported by many previous studies [e.g., *Anderson et al.*, 1992; *Meredith et al.*, 2003; *Halford et al.*, 2010, *Clausen et al.*, 2011; *Keika et al.*, 2013]. Ring current ions and/or plasma sheet ions drifting westward are considered to be the source of EMIC instability [e.g., *Anderson et al.*, 1992; *Halford et al.*, 2010], and the enhanced cold plasma density is considered to reduce the instability threshold of the EMIC wave generation [e.g., *Cornwall et al.*, 1970; *Kozyra et al.*, 1984]. Thus, the postnoon sector, in which plasmaspheric bulge or plume extending outward from the plasmasphere is formed [*Borovsky et al.*, 2014], is expected to be a favored region for EMIC wave generation during disturbed geomagnetic conditions.

Under quiet geomagnetic conditions ($Kp \leq 1$), however, the dominant region of EMIC wave occurrence is shifted toward early local times with a peak around noon as shown in Figures 9 and 10. From a comparison of the MLT occurrences obtained in both the all-*Kp* and $Kp = 0–1$ cases, we suggest that the source and generation mechanisms of quiet time EMIC waves may be different from those of EMIC waves under moderate or disturbed geomagnetic conditions.

As mentioned above, EMIC wave onsets and/or intensifications are associated with magnetospheric convection enhancement (i.e., internal source) or P_{sw} enhancement (i.e., external source). Thus, we need to know the magnetospheric and solar wind conditions for quiet time EMIC wave onset. To investigate whether quiet time EMIC waves have a causal relationship with the internal source or external source, we performed a superposed epoch analysis of 10 min averaged solar wind flow speed (V_{sw}), density (N_{sw}), dynamic pressure (P_{sw}), and IMF B_z parameters and geomagnetic indices (*AE* and *SYM-H*) for the start time EMIC wave events occurred in a region of 0800–1400 MLT. The results are shown in Figure 11. In this analysis we choose the onset time of the event as the zero epoch time ($T_E = 0$). In each panel the thick solid line indicates the median, and the lower and upper quartiles are given by the thin solid lines.

Clausen et al. [2011] reported that an increase (decrease) in *AE* (*Dst*) starting about 12 h (6 h) prior to EMIC wave onset for the all-*Kp* case. To compare with the previous results, we examined solar wind parameters and geomagnetic indices obtained at $T_E > -12$ h. Since we used the 10 min averaged solar wind data propagated from the upstream spacecraft location to the subsolar point on the bow shock [*King and Papitashvili*, 2006], sudden variations in solar wind parameters and geomagnetic indices less than 10 min are smoothed out in the superposed epoch analysis. Therefore, it should be focused on preferential solar wind and geomagnetic conditions for wave occurrence rather than a temporal wave occurrence directly driven by a sudden change in external or internal parameters.

The median values of V_{sw} in Figure 11a are constant near ~350 km/s throughout the 24 epoch hours. However, N_{sw} medians in Figure 11b gradually increase from ~4 cm^{-3} at $T_E = -12$ h to ~6 cm^{-3} at $T_E = 0$, causing P_{sw} increase. That is, the P_{sw} increase is mainly due to the N_{sw} increase. Although the median values of P_{sw} shown in Figure 11c are small, the medians clearly increase from 1.1 nPa at $T_E = -12$ h to 1.5 nPa at $T_E = 0$ indicated by the horizontal dashed line and stay at an enhanced level for several hours. This indicates that the magnetosphere is more compressed at $T_E \geq 0$ than at $T_E < 0$. Since P_{sw} enhancement causes an increase in temperature anisotropy of the trapped ring current ions in the compressed magnetosphere, the particle anisotropy leads growth of EMIC waves [e.g., *Olson and Lee*, 1983; *Anderson and Hamilton*, 1993]. Thus, we suggest that the plasma is more unstable to EMIC wave at $T_E \geq 0$ than at $T_E < 0$. Note that the lower quartile P_{sw} is nearly flat, indicating that some events occurred under steady magnetospheric conditions without P_{sw} variations (see Figure 4).

In order to discuss whether quiet time EMIC waves have a causal relationship with internal source, substorm and ring current activities before EMIC wave onset should be investigated because both activities provide hot and anisotropic ions driving the EMIC instability. In Figures 11d and 11e, the *AE* and *SYM-H* indices are plotted to indicate substorm and ring current activities, respectively. The median *AE* value increases from 21 nT at $T_E = -12$ h to 40 nT at $T_E = -5.5$ h and then decrease to 32 nT at $T_E = 0$. These *AE* values before $T_E = 0$ are too small to expect a typical substorm activity. The variation of *AE* over 24 h shown in Figure 11d is significantly different from GOES observations made for all *Kp* by *Clausen et al.* [2011]. In their study the *AE* peak of around 100 nT occurs near $T_E = 0$, nearly coincident with the peak of P_{sw}, and the *Dst* index started to decrease about 6 h prior to the EMIC wave onset. Thus, they considered both internal and external sources for EMIC wave excitation. We note that the median *AE* value at $T_E = 0$ for $Kp = 0-1$ is about 70% smaller than that for all *Kp*. The median *SYM-H* values in Figure 11e show no ring current enhancement before the onset of quiet time EMIC waves. These low levels of *AE* and *SYM-H* indices are due to IMF B_z, which is not biased toward southward, as shown in Figure 11f. At $T_E \leq 0$, the median IMF B_z values are slightly northward. This indicates that solar-wind-driven convection in the magnetosphere is not well developed before the onset of quiet time EMIC waves. From this superposed epoch analysis we suggest that solar wind dynamic pressure variation is a more important parameter than *AE* and *SYM-H* for quiet time EMIC waves occurrence in a region from morning (~0600 MLT) to afternoon (~1600 MLT).

We observed that the occurrence rate of quiet time EMIC waves is higher in the prenoon sector than in the postnoon sector. That is, there is the morning-afternoon asymmetry of the wave occurrence rate. In this study we considered P_{sw} variations as a major factor for EMIC wave occurrence during quiet geomagnetic conditions. Then, geosynchronous magnetic fields in the prenoon sector should be more sensitive to a change in P_{sw} than in the postnoon sector. Recently, we reported that the normalized sudden commencement amplitudes in the prenoon sector (MLT = 0900–1200) are larger than those in the postnoon sector (MLT = 1200–1500) at geosynchronous orbit [see *Park et al.*, 2012, Figure 4]. This indicates that the prenoon sector is more compressed than in the postnoon sector at geosynchronous orbit. Thus, the plasmas in the prenoon sector are

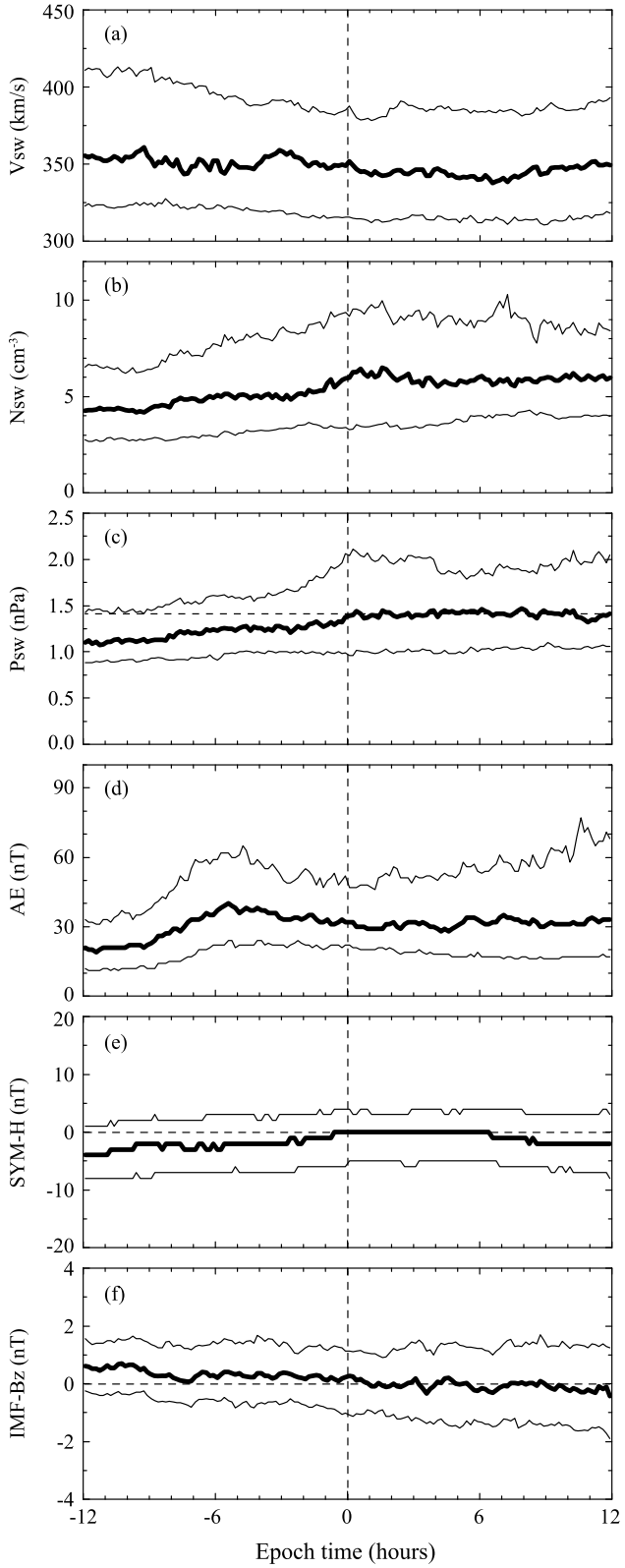

Figure 11. Superposed epoch analysis of 10 min averaged (a) solar wind flow speed (V_{sw}), (b) density (N_{sw}), (c) dynamic pressure (P_{sw}), (d) *AE*, (e) *SYM-H*, and (f) IMF B_z for the start time EMIC wave events occurred in a region of 0800–1400 MLT. The zero epoch time indicated by dashed line in each panel is given as the onset time of the event. The horizontal dashed line in Figure 11c indicates the value of P_{sw} at the onset.

more unstable to EMIC waves than those in the postnoon sector during the response of the geosynchronous magnetic field to solar wind dynamic pressure variations.

5. Conclusion

We have examined the local time occurrence distribution of the quiet time EMIC waves observed at geosynchronous orbit during solar minimum year 2007–2008. Unlike previous studies, which reported high EMIC wave occurrence in the postnoon sector with a peak around 1500–1600 MLT during disturbed geomagnetic conditions, we observed that quiet time EMIC waves mostly occur in a region from morning to afternoon with a peak occurrence near noon. To investigate whether the quiet time EMIC waves have a causal relationship with magnetospheric convection enhancement or solar wind dynamic pressure variations, we performed a superposed epoch analysis of solar wind parameters (P_{sw} and IMF B_z) and geomagnetic (*AE* and *SYM-H*) indices. We found that the major driver of geosynchronous quiet time EMIC waves is solar wind pressure variations. This result is consistent with THEMIS observations by *Usanova et al.* [2012]. It has been suggested that EMIC waves can resonate with relativistic electrons and cause loss of relativistic electrons into the Earth's atmosphere through pitch angle scattering. Recently, *Hyun et al.* [2014] reported that EMIC waves play a significant role in the electron flux dropout under quiet geomagnetic conditions. Until now, however, no statistical study has been reported for the relationship between quiet time EMIC wave occurrence and relativistic electron flux variations. In the near future we will do statistical analyses to examine whether EMIC waves mainly contribute to the variations of the electron flux during quiet times.

Acknowledgments

The high time resolution GOES magnetic field data were provided from coordinated data analysis web (CDAWeb), http://cdaweb.gsfc.nasa.gov/cdaweb. The geomagnetic indices (*Kp*, *AE*, and *SYM-H*) were provided by the World Data Center C2 (WDC-C2) for Geomagnetism, Kyoto University (http://wdc.kugi.kyoto-u.ac.jp/index.html). The solar wind and interplanetary magnetic field (IMF) data were obtained from OMNI Web (http://omniweb.gsfc.nasa.gov/). This work was supported by BK21+ through the National Research Foundation (NRF) funded by the Ministry of Education of Korea. Work of K.-H. Kim was supported by the Basic Science Research Program through NRF funded by NRF-2013R1A1A2A10004414 and also supported by project PE15090 of Korea Polar Research Institute. This work was supported by JSPS KAKENHI Grant Number 15H05815.

References

Anderson, B. J., R. E. Erlandson, and L. J. Zanetti (1992), A statistical study of Pc 1–2 magnetic pulsations in the equatorial magnetosphere: 1. Equatorial occurrence distributions, *J. Geophys. Res.*, *97*(A3), 3075–3088, doi:10.1029/91JA02706.

Anderson, B. J., and D. C. Hamilton (1993), Electromagnetic ion cyclotron waves stimulated by modest magnetospheric compressions, *J. Geophys. Res.*, *98*(A7), 11,369–11,382, doi:10.1029/93JA00605.

Arnoldy, R. L., et al. (2005), Pc1 waves and associated unstable distributions of magnetospheric protons observed during a solar wind pressure pulse, *J. Geophys. Res.*, *110*, A07229, doi:10.1029/2005JA011041.

Borovsky, J. E., D. T. Welling, M. F. Thomsen, and M. H. Denton (2014), Long-lived plasmaspheric drainage plumes: Where does the plasma come from?, *J. Geophys. Res.*, *119*, 6496–6520, doi:10.1002/2014JA020228.

Clausen, L. B. N., J. B. H. Baker, J. M. Ruohoniemi, and H. J. Singer (2011), EMIC waves observed at geosynchronous orbit during solar minimum: Statistics and excitation, *J. Geophys. Res.*, *116*, A10205, doi:10.1029/2011JA016823.

Cornwall, J. M. (1965), Cyclotron instabilities and electromagnetic emission in the ultra low frequency and very low frequency ranges, *J. Geophys. Res.*, *70*(1), 61–69, doi:10.1029/JZ070i001p00061.

Cornwall, J. M., F. V. Coroniti, and R. M. Thorne (1970), Turbulent loss of ring current protons, *J. Geophys. Res.*, *75*(25), 4699–4709, doi:10.1029/JA075i025p04699.

Engebretson, M. J., et al. (2002), Observations of two types of Pc 1–2 pulsations in the outer dayside magnetosphere, *J. Geophys. Res.*, *107*(A12), 1451, doi:10.1029/2001JA000198.

Erlandson, R. E., and A. J. Ukhorskiy (2001), Observations of electromagnetic ion cyclotron waves during geomagnetic storms: Wave occurrence and pitch angle scattering, *J. Geophys. Res.*, *106*(A3), 3883–3895.

Fraser, B. J., and R. L. McPherron (1982), Pc 1–2 magnetic pulsation spectra and heavy ion effects at synchronous orbit: ATS 6 results, *J. Geophys. Res.*, *87*(A6), 4560–4566, doi:10.1029/JA087iA06p04560.

Fraser, B. J., and T. S. Nguyen (2001), Is the plasmapause a preferred source region of electromagnetic ion cyclotron waves in the magnetosphere?, *J. Atmos. Sol. Terr. Phys.*, *63*, 1225–1247.

Fraser, B. J., R. S. Grew, S. K. Morley, J. C. Green, H. J. Singer, T. M. Loto'aniu, and M. F. Thomsen (2010), Storm time observations of electromagnetic ion cyclotron waves at geosynchronous orbit: GOES results, *J. Geophys. Res.*, *115*, A05208, doi:10.1029/2009JA014516.

Fraser, B. J., S. K. Morley, R. S. Grew, and H. J. Singer (2012), Classification of Pc1-2 electromagnetic ion cyclotron waves at geosynchronous orbit, in *Dynamics of the Earth's Radiation Belts and Inner Magnetosphere, Geophys. Monogr. Ser.*, vol. 199, pp. 53–68, AGU, Washington, D. C., doi:10.1029/2012GM001353.

Goldstein, J., B. R. Sandel, M. F. Thomsen, M. Spasojević, and P. H. Reiff (2004), Simultaneous remote sensing and in situ observations of plasmaspheric drainage plumes, *J. Geophys. Res.*, *109*, A03202, doi:10.1029/2003JA010281.

Halford, A. J., B. J. Fraser, and S. K. Morley (2010), EMIC wave activity during geomagnetic storm and nonstorm periods: CRRES results, *J. Geophys. Res.*, *115*, A12248, doi:10.1029/2010JA015716.

Horne, R. B., and R. M. Thorne (1994), Convective instabilities of electromagnetic ion cyclotron waves in the outer magnetosphere, *J. Geophys. Res.*, *99*(A9), 17,259–17,273.

Hu, Y. D., and B. J. Fraser (1994), Electromagnetic ion cyclotron wave amplification and source regions in the magnetosphere, *J., Geophys. Res.*, *99*(A1), 263–272.

Hyun, K., K.-H. Kim, E. Lee, H.-J. Kwon, D.-H. Lee, and H. Jin (2014), Loss of geosynchronous relativistic electrons by EMIC wave scattering under quiet geomagnetic conditions, *J. Geophys. Res. Space Physics*, *119*, 8357–8371, doi:10.1002/2014JA020234.

Ishida, J., S. Kokubun, and R. L. McPherron (1987), Substorm effects on spectral structures of Pc 1 waves at synchronous orbit, *J. Geophys. Res.*, *92*(A1), 143–158.

Keika, K., K. Takahashi, A. Y. Ukhorskiy, and Y. Miyoshi (2013), Global characteristics of electromagnetic ion cyclotron waves: Occurrence rate and its storm dependence, *J. Geophys. Res. Space Physics*, *118*, 4135–4150, doi:10.1002/jgra.50385.

Kennel, C. F., and H. E. Petschek (1966), Limit on stably trapped particle fluxes, *J. Geophys. Res.*, *71*(1), 1–28.

Kim, K.-H., J. Goldstein, and D. Berube (2007), Plasmaspheric drainage plume observed by the Polar satellite in the prenoon sector and the IMAGE satellite during the magnetic storm of 11 April 2001, *J. Geophys. Res.*, *112*, A06237, doi:10.1029/2006JA012030.

King, J., and N. Papitashvili (2006), *One Min and 5-Min Solar Wind Data Sets at the Earth's Bow Shock Nose*, NASA/Goddard Space Flight Cent., Greenbelt, Md.

Kozyra, J. U., T. E. Cravens, F. Nagy, E. G. Fontheim, and R. S. B. Ong (1984), Effects of energetic heavy ions on electromagnetic ion cyclotron wave generation in the plasmapause region, *J. Geophys. Res.*, *89*(A4), 2217–2233, doi:10.1029/JA089iA04p02217.

Kwon, H.-J., K.-H. Kim, G. Jee, J.-S. Park, H. Jin, and Y. Nishimura (2015), Plasmapause location under quiet geomagnetic conditions ($Kp \leq 1$): THEMIS observations, *Geophys. Res. Lett.*, *42*, 7303–7310, doi:10.1002/2015GL066090.

McCollough, J. P., S. R. Elkington, M. E. Usanova, I. R. Mann, D. N. Baker, and Z. C. Kale (2010), Physical mechanisms of compressional EMIC wave growth, *J. Geophys. Res.*, *115*, A10214, doi:10.1029/2010JA015393.

Meredith, N. P., R. M. Thorne, R. B. Horne, D. Summers, B. J. Fraser, and R. R. Anderson (2003), Statistical analysis of relativistic electron energies for cyclotron resonance with EMIC waves observed on CRRES, *J. Geophys. Res.*, *108*(A6), 1250, doi:10.1029/2002JA009700.

Min, K., J. Lee, K. Keika, and W. Li (2012), Global distribution of EMIC waves derived from THEMIS observations, *J. Geophys. Res.*, *117*, A05219, doi:10.1029/2012JA017515.

Miyoshi, Y., K. Sakaguchi, K. Shiokawa, D. Evans, J. Albert, M. Connors, and V. Jordanova (2008), Precipitation of radiation belt electrons by EMIC waves, observed from ground and space, *Geophys. Res. Lett.*, *35*, L23101, doi:10.1029/2008GL035727.

O'Brien, T. P., and M. B. Moldwin (2003), Empirical plasmapause models from magnetic indices, *Geophys. Res. Lett.*, *30*(4), 1152, doi:10.1029/2002GL016007.

Olson, J. V., and L. C. Lee (1983), Pc1 wave generation by sudden impulses, *Planet. Space Sci.*, *31*(3), 295–302, doi:10.1016/0032-0633(83)90079-X.

Park, J.-S., K.-H. Kim, D.-H. Lee, T. Araki, E. Lee, and H. Jin (2012), Statistical analysis of SC-associated geosynchronous magnetic field perturbations, *J. Geophys. Res.*, *117*, A09212, doi:10.1029/2012JA017648.

Roux, A., S. Perraut, J. L. Rauch, C. de Villedary, G. Kremser, A. Korth, and D. T. Young (1982), Wave-particle interactions near Ω_{He^+} observed on board GEOS 1 and 2: 2. Generation of ion cyclotron waves and heating of He^+ ions, *J. Geophys. Res.*, *87*(A10), 8174–8190, doi:10.1029/JA087iA10p08174.

Singer, H., L. Matheson, R. Grubb, A. Newman, and D. Bouwer (1996), Monitoring space weather with the GOES magnetometers, in *Society of Photo-Optical Instrumentation Engineers (SPIE) Conference Series*, vol. 2812, edited by E. R. Washwell, pp. 299–308, Soc. of Photo-Opt. Instrum. Eng., Bellingham, Wash.

Spasojević, M., J. Goldstein, D. L. Carpenter, U. S. Inan, B. R. Sandel, M. B. Moldwin, and B. W. Reinisch (2003), Global response of the plasmasphere to a geomagnetic disturbance, *J. Geophys. Res.*, *108*(a9), 1340, doi:10.1029/2003JA009987.

Summers, D., and R. M. Thorne (2003), Relativistic electron pitch-angle scattering by electromagnetic ion cyclotron waves during geomagnetic storms, *J. Geophys. Res.*, *108*(A4), 1143, doi:10.1029/2002JA009489.

Thorne, R. M., and C. F. Kennel (1971), Relativistic electron precipitation during magnetic storm main phase, *J. Geophys. Res.*, *76*(19), 4446–4453, doi:10.1029/JA076i019p04446.

Usanova, M. E., I. R. Mann, I. J. Rae, Z. C. Kale, V. Angelopoulos, J. W. Bonnell, K. H. Glassmeier, H. U. Auster, and H. J. Singer (2008), Multipoint observations of magnetospheric compression-related EMIC Pc1 waves by THEMIS and CARISMA, *Geophys. Res. Lett.*, *35*, L17S25, doi:10.1029/2008GL034458.

Usanova, M. E., I. R. Mann, J. Bortnik, L. Shao, and V. Angelopoulos (2012), THEMIS observations of electromagnetic ion cyclotron wave occurrence: Dependence on AE, SYMH, and solar wind dynamic pressure, *J. Geophys. Res.*, *117*, A10218, doi:10.1029/2012JA018049.

Young, D. T., S. Perraut, A. Roux, C. de Villedary, R. Gendrin, A. Korth, G. Kremser, and D. Jones (1981), Wave-particle interactions near Ω_{He^+} observed on GEOS 1 and 2: 1. Propagation of ion cyclotron waves in He^+-rich plasma, *J. Geophys. Res.*, *86*(A8), 6755–6772, doi:10.1029/JA086iA08p06755.

Yuan, Z., Y. Xiong, D. Wang, M. Li, X. Deng, A. G. Yahnin, T. Raita, and J. Wang (2012), Characteristics of precipitating energetic ions/electrons associated with the wave-particle interaction in the plasmaspheric plume, *J. Geophys. Res.*, *117*, A08324, doi:10.1029/2012JA017783.